This study investigates air flow characteristics and the temperature field in the combustion chamber, which are determined by the geometry of the swirler. The task addressed is predetermined by the fact that swirlers manufactured by conventional casting methods with subsequent assembly are characterized by significant geometric deviations of the flow-through elements. This leads to a dispersion of air flow along the contours, a violation of the uniformity of the fuel-air mixture and, as a result, to increased circular unevenness of the temperature field at the outlet of the combustion chamber, which reduces the resource and reliability of engine operation.

In this work, three-dimensional simulation of the swirler was performed using the Unigraphics NX CAD system; a numerical CFD analysis of processes in the combustion chamber was carried out. Experimental studies on geometric deviations and air flow rates for swirlers manufactured by the conventional casting method and the additive method L-PBF (Laser Powder Bed Fusion) were conducted. The geometric accuracy was assessed using a 3-D scanning method with comparison with a digital model; the flow characteristics were determined by bench tests during the purging of the air and fuel circuits, as well as during the combined operation of the circuits.

It was found that the swirlers manufactured using the L-PBF method provide air flow stability within ±1.5%, which is a better indicator compared to cast analogs. That has made it possible to reduce the circular unevenness of the combustion chamber temperature field to 12.5–18.9% with an allowable value of no more than 21%.

The results confirm the feasibility of using additive technologies for the manufacture of swirlers for combustion chambers in gas turbine engines

Keywords: additive technologies, L-PBF, swirler, combustion chamber, gas turbine engine, CFD simulation

UDC 621.452.3.036:621.762.5:621.9.048
DOI: 10.15587/1729-4061.2026.359455

DESIGN OF A CONSOLIDATED SWIRLER MONOPART STRUCTURE BY OPTIMIZING THE PROCESSES OF MICROMETALLURGICAL LAYER-TO-LAYER FUSION OF HEAT-RESISTANT ALLOYS

Volodymyr Yefanov
Doctor of Philosophy (PhD), Deputy Director
Scientific and Educational Institute "Titan"*
ORCID: https://orcid.org/0000-0002-6363-4081
Oleh Kalinichenko
Corresponding author
PhD
Department of Fuel, Polymer,
and Polygraphic Materials Technologies*
E-mail: kalinichenkooleg1@gmail.com
ORCID: https://orcid.org/0000-0001-5597-6084
Dmytro Kuts
PhD Student
Department of Power Engineering*
ORCID: https://orcid.org/0009-0000-3110-4978
Oleh Ovchynnykov
Department of Fuel, Polymer,
and Polygraphic Materials Technologies*
ORCID: https://orcid.org/0009-0005-3172-0582
Hanna Laptieva
PhD
Department of Integrated Technologies
of Welding and Modeling of Structures
National University Zaporizhzhia Polytechnic
Universytetska str., 64, Zaporizhia, Ukraine, 69063
ORCID: https://orcid.org/0000-0003-4475-2354
*Ukrainian State University of Science and Technologies
Lazaryana str., 2, Dnipro, Ukraine, 49010

Received 28.01.2026
Received in revised form 18.03.2026
Accepted 15.04.2026
Published 30.04.2026

How to Cite: *Yefanov, V., Kalinichenko, O., Kuts, D., Ovchynnykov, O., Laptieva, H. (2026). Design of a consolidated swirler monopart structure by optimizing the processes of micrometallurgical layer-to-layer fusion of heat-resistant alloys. Eastern-European Journal of Enterprise Technologies, 2 (1 (140)), 91–104. https://doi.org/10.15587/1729-4061.2026.359455*

1. Introduction

The efficiency and reliability of modern aircraft gas turbine engines (AGTEs) are largely determined by the quality of gas-dynamic processes occurring in the combustion chambers. These processes involve complex interactions between turbulent flow, fuel delivery, chemical combustion reactions, and heat transfer. Their adequate modeling is key to ensuring stable engine operation, reducing nitrogen oxide (NO_x) emissions, and improving fuel efficiency [1, 2].

Among the numerous methods, the use of turbulent modeling (e.g., Reynolds-Averaged Navier-Stokes, Large Eddy Simulation) in combination with combustion models, such as Flamelet Generated Manifold (FGM) or Eddy Dissipation Concept (EDC) [3, 4], is particularly common. These models allow for accurate reproduction of local features of the

combustion flame, in particular, the behavior in the zone of influence of vortices, which are key elements for the formation of the flow structure and flame stabilization [5].

A large number of products specializing in computational aero hydrodynamics have been developed, making the analysis of individual aspects of the combustion process using computational aero hydrodynamics methods a common practice in engine engineering.

The design of the swirler directly affects the formation of toroidal vortices that hold the flame in the center of the combustion chamber, ensuring the necessary degree of mixing of the fuel with the oxidant. Conventional manufacturing methods, such as casting, stamping, and machining, have limitations in the implementation of complex geometries, which negatively affects the potential for design optimization [6].

The use of additive technologies, in particular selective laser melting (L-PBF) or electron beam melting (EBM), opens up new possibilities for manufacturing parts with complex topologies with high accuracy and a minimum number of joints [7]. However, the surface roughness, porosity, and residual stresses inherent in parts manufactured using 3D printing can affect the aerodynamic flow characteristics and thermal stability of components [8, 9].

Research in the field of additive manufacturing of parts shows that this technology, with simultaneous hot isostatic pressing (HIP) [5, 6], is capable of ensuring the serial production of AGTE parts with the required level of accuracy and physical and mechanical properties.

According to the results reported in [10], it was found that HIP with subsequent heat treatment contributes to the almost complete "healing" of pores and microcracks, which are concentrated in the internal volumes of the metal, and in the "healing" zone, globular and (or) film oxides are detected. The microstructure of the samples is characteristic of the normal heat-treated state of the Inconel 718 alloy, and overheating is not observed. In the material of the studied samples, after hot isostatic pressing with subsequent heat treatment, lamellar δ-phases are isolated, with carbides and carbonitrides being isolated mainly in the form of discrete globular particles.

The advantages of using the additive method for AGTE parts are in reducing the time for manufacturing parts and the associated costs, the possibility of designing and manufacturing complex geometry, which provides lightness, combining several components and increasing productivity [9, 10].

That is why designing the structure of aircraft engine swirlers as a single part is an urgent scientific and practical task, which is of critical importance for the development of civil and defense aircraft manufacturing.

2. Literature review and problem statement

In [1, 2], the influence of the geometry of swirlers on the formation of the recirculation zone and flame stabilization is described, while it is established that the geometric parameters significantly affect the mixing efficiency, air and fuel, but the issue of ensuring the required accuracy of their manufacture is not fully developed. In addition, the use of LES models for detailed analysis of the flame structure is considered [3, 4], which makes it possible to increase the accuracy of calculations; however, significant computational costs limit the use of this approach in practice. In work [5], the results of studies on gas-dynamic processes in combustion chambers of aircraft gas turbine engines using numerical modeling are reported. It is shown that the use of RANS approaches makes it possible to obtain acceptable accuracy of prediction of temperature and velocity fields of the flow; however, the accuracy of turbulent structures in the swirler zone remains limited.

Much attention has been paid to experimental studies [5], which provide information that even minor deviations in the geometry of combustion chamber elements, in particular swirlers, lead to significant uneven distribution of the temperature field in the engine, which negatively affects its resource; however, the reasons for such deviations are mostly related to the manufacturing technology and remain insufficiently studied. Conventional technologies for manufacturing combustion chamber parts [6, 7], such as casting with subsequent machining, have been analyzed. In the cited works, issues related to the limitations of reproducing the complex internal geometry of the swirler remained unresolved. This is an objective reason that hinders the possibility of optimizing the design.

All this allows us to argue that it is advisable to conduct research on more promising manufacturing technologies, namely additive technologies. Thus, it has been shown that the selective laser melting technology [8] allows the manufacture of parts of complex geometry with high accuracy and a minimum number of joints; however, problems associated with porosity and residual stresses of the material remain. It has been established that the use of hot isostatic pressing (HIP) allows for a significant reduction in the number of internal defects and an increase in the density of the material [9, 10]; however, the influence of HIP on the operational characteristics of combustion chamber parts under real-world conditions has not been sufficiently studied.

A comprehensive approach to combining numerical modeling and additive manufacturing [11, 12] shows that the integration of these methods allows for increased efficiency of structures, but there are no generalized methods that take into account both gas-dynamic and technological factors. It should be noted that the surface roughness [13], which is characteristic of additive manufacturing of parts, can significantly affect both the flow structure and pressure loss in the chamber, but the ways to reduce it without significantly increasing costs remain an open question.

All this gives grounds to argue that it is advisable to conduct a study aimed at optimizing the geometry of the swirler itself using numerical modeling, while taking into account the possibility of improving the mixing of fuel and air. In this case, attention should be paid to expanding the technological capabilities of manufacturing parts.

3. The aim and objectives of the study

The aim of our work is to design a consolidated swirler structure for further optimization of the processes of micrometallurgical layer-by-layer fusion of heat-resistant alloys as monocomponents. This will make it possible to significantly reduce the number of defects and increase the accuracy of geometry, improve high strength and durability, as well as mechanical properties of monocomponents.

To achieve the goal, the following tasks were set:

– to construct a precision three-dimensional swirler model in the Unigraphics NX environment that takes into account the complex geometric features of air contours;

– to conduct a comparative analysis of the geometric accuracy of swirler blades manufactured using casting technology and the L-PBF method, using the 3D scanning method, and to establish the influence of geometric deviations on the stability of air flow characteristics, to determine the level of technological defects;

– to investigate the influence of hot isostatic pressing on the porosity and microstructure of the material of additively manufactured swirlers.

4. The study materials and methods

The object of our study is the air flow characteristics and the temperature field of the combustion chamber, which are determined by the geometry of the swirler. The hypothesis of the study assumes that the use of additive technology of laser powder bed melting (L-PBF) provides higher geometric accuracy of swirlers compared to conventional casting technologies, which, in turn, leads to stabilization of air flow characteristics and improvement of the temperature field of the combustion chamber.

A number of assumptions were adopted during the study. The working fluid was considered as a compressible ideal gas, the combustion process was modeled in a stationary setting, and the heat transfer through the outer walls was considered adiabatic. The material properties were assumed to be isotropic.

In order to simplify the numerical analysis, the geometry of the model was adapted by removing secondary structural elements that do not have a significant impact on gas-dynamic processes. In addition, a sector model of the combustion chamber was used, which allowed us to reduce computational costs while maintaining the representativeness of results.

The sequence of numerical calculations for determining the characteristics of combustion chambers in the ANSYS Fluent program consisted of five main stages:

– construction of a solid-state mathematical model of the flow in the combustion chamber;

– construction of a computational grid of the above-mentioned solid-state model;

– setting the boundary conditions of the model and setting the solver;

– calculation;

– post-processing of the results.

Based on the drawings, a solid-state model of the entire combustion chamber was constructed. The solid-state model obtained in this way serves as the basis for building a solid-state model of the part of the flow (domain) in which the working fluid flows.

At the second stage of the technological process, a grid was generated on the computational model. The boundary conditions task involves determining the working fluid, for example, air or an ideal gas, a turbulence model, interaction between computational grids, flow parameters at the inlet and outlet of the combustion chamber, heat exchange of the air flow with the walls, etc.

In this case, the modified Navier-Stokes equation was used, supplemented by the Menter k-ω SST (Shear Stress Transport) model (1.2, 1.3), which is a two-equation model that combines the advantages of k-ε and k-ω. It is often used in combustion models, especially for complex turbulence configurations, and is based on solving the transport equations for:

– k – turbulent kinetic energy, (m^2/s^2);

– ω – specific dissipation of turbulent energy, (1/s).

These equations are described by the following dependences:

– momentum equation (Navier-Stokes)

$$\rho\left(\frac{\partial u_i}{\partial t}+u_j\frac{\partial u_i}{\partial x_j}\right)=-\frac{\partial p}{\partial x_i}+\frac{\partial}{\partial x_j}\left[\left(\mu+\mu_t\right)\left(\frac{\partial u_i}{\partial x_j}+\frac{\partial u_j}{\partial x_i}\right)\right], \quad (1)$$

where μ is dynamic, (Pa · s); μ_t is turbulent viscosity, (Pa · s)

$$\mu_t=\rho\frac{k}{\omega};$$

u_i – velocity components in the coordinate direction, m/s; u_j – velocity vector component corresponding to the transfer (mass, momentum, energy) in the x_j direction; x_i – spatial coordinates; t – time, s; p – pressure, Pa (N/m^2); ρ – density, kg/m^3;

– equation for k – turbulent kinetic energy

$$\frac{\partial\left(\rho k\right)}{\partial t}+\frac{\partial\left(\rho u_j k\right)}{\partial x_j}=$$
$$=P_k-\beta^*\rho k\omega+\frac{\partial}{\partial x_j}\left[\left(\mu+\sigma_k\mu_t\right)\frac{\partial_k}{\partial x_j}\right], \quad (2)$$

where k is the turbulent kinetic energy, m^2/s^2; P_k is the turbulent energy production (usually due to shear), kg/m · s^3

$$P_k=\tau_{ij}\frac{\partial u_i}{\partial x_j},$$

β^*, σ_k – dimensionless coefficient/constant;

– equation for ω – specific dissipation rate

$$\frac{\partial\left(\rho\omega\right)}{\partial t}+\frac{\partial\left(\rho u_j\omega\right)}{\partial x_j}=\alpha\frac{\omega}{k}P_k-\beta\rho\omega^2+$$
$$+\frac{\partial}{\partial x_j}\left[\left(\mu+\sigma_\omega\mu_t\right)\frac{\partial\omega}{\partial x_j}\right]+2\left(1-F_1\right)\rho\sigma_{\omega^2}\frac{1}{\omega}\frac{\partial k}{\partial x_j}\frac{\partial\omega}{\partial x_j}, \quad (3)$$

where ω is the specific rate of turbulent energy dissipation, 1/s; F_1 is the mixing function that provides a smooth transition between models; μ_t is the turbulent (effective) viscosity, Pa · s

$$\mu_t=\frac{\rho k}{\max\left(\omega,F_2SF_{\text{lim}}\right)},$$

F_2 – transition function between flow zones; S – modulus of the strain rate tensor, 1/s; α, β, σ_ω, σ_ω^2 – empirical constant models; F_{lim} – limiting function.

Post-processing of the results in the numerical experiment is the final stage. At this stage, the degree of inconsistency of the convergence of the equations of the conducted experiment was first determined, that is, the degree of its divergence by at least three orders of magnitude, which corresponds to sufficient convergence. Most attention was paid to temperature fields, assessment of combustion efficiency, and possible zones of formation of toxic components.

Thanks to the wide capabilities of the software product used, in addition to numerical results, we also received a graphic visualization of the calculations performed, such as pressure, velocity, temperature distribution fields, etc. in any planes of interest to us. Color contour temperature maps allow us to determine the shape, length, and position of the flame. This helps identify zones of enrichment or incomplete combustion, as well as potential areas of formation of harmful emissions. Vector velocity fields and vortex contours allow us to understand how the flow is distributed in the chamber, where recirculation zones necessary for flame stabilization arise. This is critical for the optimal location of the injectors and the selection of ignition conditions. Wall and gas temperature maps provide a visual representation of the inhomogeneity of thermal fields, which allows preventing local overheating of the chamber walls or reducing combustion

efficiency due to insufficient heating. Visualization of fuel and air mass fractions makes it possible to assess the mixing efficiency to improve the geometry of swirlers or injectors.

In this work, three-dimensional models of combustion chamber parts were built using the drawings (Fig. 1) in the Unigraphics NX CAD program (USA).

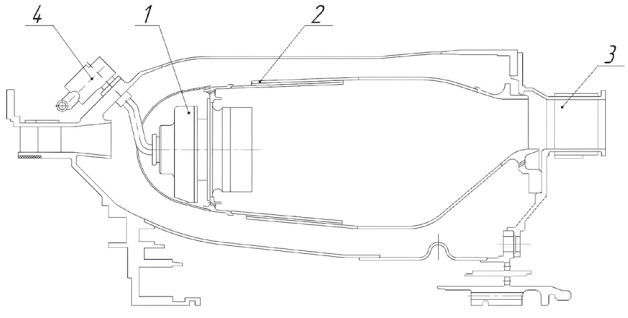

Fig. 1. Longitudinal cross-section of the combustion chamber: 1 — swirler; 2 — flame tube; 3 — nozzle apparatus; 4 — additional fuel collector

Three-dimensional models correspond to the real design of the object with existing fillets, bolted joints, and radiuses of curvature, which significantly complicate the process of meshing and decomposition.

The geometry of the mathematical model of the combustion chamber flow corresponds to the simplified design of the real object; therefore, to build the flow model, an appropriate simplified model of the combustion chamber parts was first prepared. After that, a longitudinal section of the solid-state mathematical model of the flow of the single-burner sector of CC was built in accordance with the simplified design of the parts.

The decomposition of the solid-state flow model makes it possible to simplify the process of constructing a mesh and specify at the stage of preparation for application accurate surfaces that can be used for calculations in post-processing (for example, air flow or average temperature, etc.).

The construction of a finite element (FE) mesh of the combustion chamber air flow for modeling combustion processes and obtaining the swirler temperature gradient was performed using the Ansys Meshing module (USA).

The computational domain of space, which includes a single-burner sector, is geometrically complex, consists of several parts and is of different scales. For this task, a polyhedral mesh was chosen since, with the same volume, it has significantly fewer elements compared to a tetrahedral mesh (Table 1); therefore, the use of a tetrahedral mesh is not rational in terms of the use of computational resources and time. Since Ansys Meshing does not make it possible to build a polyhedral mesh, the tetrahedral mesh was converted to a polyhedral mesh in Fluent itself.

Table 1

Parameters of different types of calculation grid

Grid type	Number of nodes, units	Number of elements, units
polyhedral	12,828,143	5,342,167
tetrahedral	14,926,255	8,607,048

For the solid model of the single-burner sector of the working fluid and the model of structural elements (solid), a separate mesh flow model (domain) was built with full correspondence of the size and shape of the mesh on the contact surfaces.

On the surface of the swirler ring, a local thickening was formed using the Inflation function of the near-wall layer.

The flow in the combustion chamber is characterized by high gradients of temperature, density, and velocity, especially in the flame zone and near the walls. Correct reproduction of the thermal boundary layer is critical for accurate heat transfer prediction; therefore, inflation regions should be used on all solid surfaces, especially in the swirler and nozzle zones.

The boundary conditions task involves determining the working fluid, for example, air or an ideal gas, a turbulence model, a combustion model, flow parameters at the inlet and outlet of the model, heat exchange of the air flow with the walls, etc. In this case, for further implementation of the experiment in the ANSYS Fluent software package, the following solver settings were selected for the constructed computational grid, which are given in Table 2.

On the inlet face (IN), the mass flow rate G_{fl}, the total temperature T^*, the turbulence intensity and the ratio of turbulent density to dynamic density were specified.

On the outlet face (OUT) – the excess pressure, the total temperature of the return flow, the intensity of the turbulent return flow and the ratio of turbulent density to dynamic density of the return flow.

On the side faces (Periodic), the type of boundary requirements Rotational-periodic was specified.

The outer walls of the fluid domain were modeled as adiabatic. The contact walls with the solid were modeled as coupled. Each solid domain (separated depending on the material) was given the following material properties:

– density (Density, kg/m^3);

– specific heat capacity C_p (SpecificHeat, J/kg-K);

– thermal conductivity λ (Thermal conductivity, W/m-K).

The calculation is performed independently, providing the display of dynamic plots of the agreement of residuals and key variables (Fig. 2) over iterations to track the convergence of the solution. The display of residual plots is provided automatically; for others, monitoring tasks are used (Monitors).

Fig. 10 shows the convergence of the equations for mass balance (continuity), velocities (x, y, z-velocity) along the axes in the Navier-Stokes equation, energy participating in heat transfer, combustion, and temperature. Turbulent parameters show the amount of energy in turbulent vortices (k) and their decay rate (ω). The parameter fmean is a post-process function. tvar is a mixture variable, temperature, or chemistry parameter for previously unmixed models.

For this calculation, surface monitoring (SurfaceMonitor) was specified over iterations to change the imbalance of mass flows at the inlet and outlet of the fluid domain, and for the temperature at the outlet of the combustion chamber in the nozzle plane (Fig. 3).

Monitoring the temperature at the outlet of the combustion chamber is set to control the convergence of the calculation with the real values of the temperature at the outlet of the combustion chamber in the plane of the nozzle apparatus.

The initial values of the calculation are the numerical values of the independent variables at the nodes of the calculation grid with unknown coordinates. The analysis of such significant volumes of numerical information in alphanumeric order is practically not feasible.

Table 2

Solver settings

Aspect of the numerical process	Mathematical description	Fluent solver option
Time	Stationary form of gas phase equations	Steady
Density	Reynolds-Favre averaged Navier-Stokes (RANS) equations, closed by a turbulence model SSTk-ω	SSTk-ω
Wall functions	Standard wall functions [11]	Standard wall Functions
Combustion and transport of chemical components	Immiscible mixture model (Schwab-Zeldovich function, probability density function, pre-calculated PFD tables). Conservation equation of the Schwab-Zel'dovich function and its variance [12–14]	Non-Premixed Combustion
Motion, heat transfer, and evaporation of atomized fuel droplets	Disperse phase model (Lagrangian equations of motion and heat and mass transfer of spherical drops) [14]	Discrete Phase Model
Effect of fuel droplets on gas	The drop-source model in the cell [15]	Interaction with Continuous Phase
Pressure-VelocityCoupling (Speed pressure correction method)	Iterative correction of the pressure field so that the resulting velocity field satisfies the continuity equation	SIMPLE
Equations (Computed equations)	Flow (4 equation)	–
	Turbulence (2 equation)	
	Energy (1 equation)	
	PDF (2 equation)	
Discretization (Discretization scheme)	1st order accuracy "against the flow"	First Order Upwind Third Order MUSCL
	3rd order Van Leer accuracy "against the flow" [16]	
Under-Relaxation (Relaxation coefficients)	Pressure – 0.2	–
	Momentum – 0.5	
	Energy – 0.9	
	Temperature – 0.9	
	Mean Mixture Fraction – 0.9	
	Mixture Fraction Variance – 0.8	
	Discrete Phase Sources – 0.2	
	Others are default	

To implement the 3D printing technology, the structural monopart described using the STL file must be decomposed into thin layers. Using the EOS RP-Tools software, the following operations are performed with the STL data:

– data format conversion;
– division into layers;
– SU data viewing;
– shell and core generation.

The result is an SLI file.

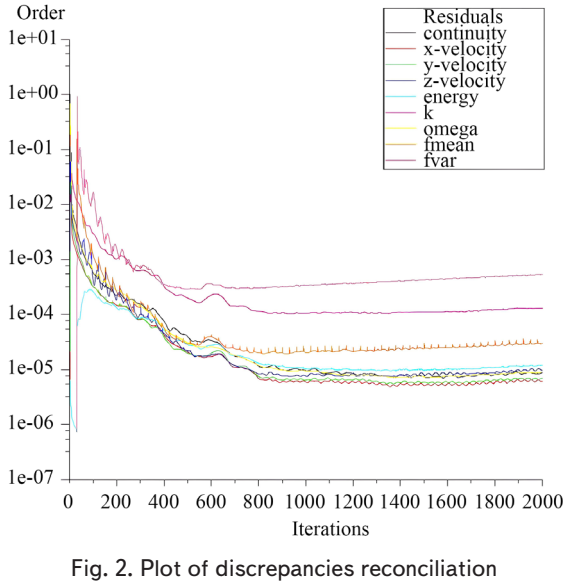

Fig. 2. Plot of discrepancies reconciliation

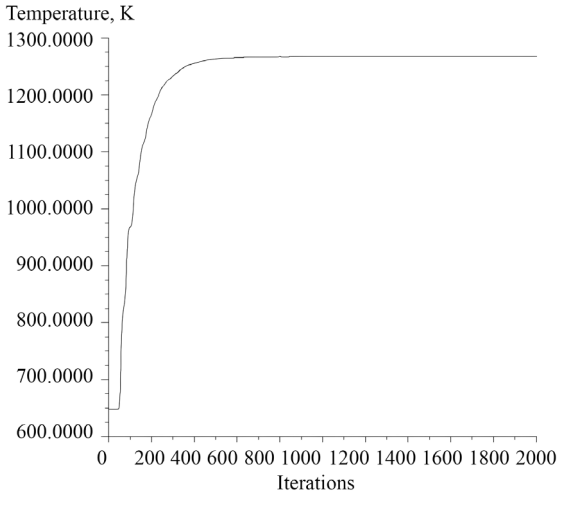

Fig. 3. Planar temperature monitoring at the combustion chamber outlet

The position of the parts on the build platform is determined. The parts are placed next to each other. Improved part layout combined with the ability to produce simultaneously can significantly reduce costs, as, depending on the part, setup and auxiliary procedures can be significantly reduced. The creation of supports helps ensure stable component fixation and heat dissipation during the L-PBF process.

5. Results of research on additive manufacturing parameters and characteristics of combustion chamber swirlers

5. 1. Results of building a three-dimensional swirler model

A precision three-dimensional swirler model was constructed in the Unigraphics NX environment, taking into account the complex geometric features of air contours (Fig. 4–7)

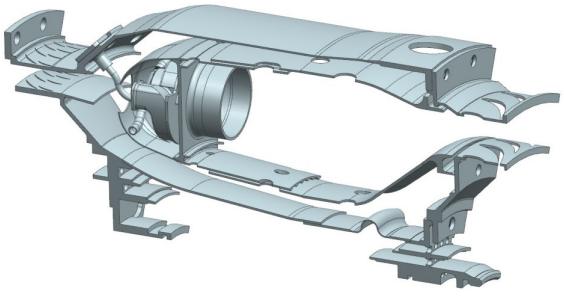

Fig. 4. Three-dimensional models of combustion chamber parts in a single-burner sector of the combustion chamber

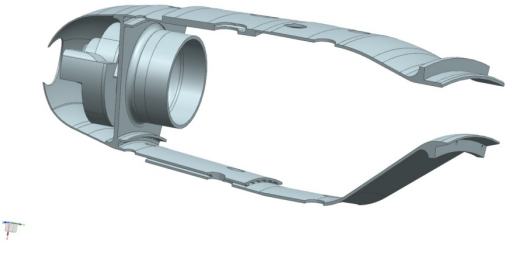

Fig. 5. Models of simplified design of combustion chamber parts in a single-burner sector of the combustion chamber

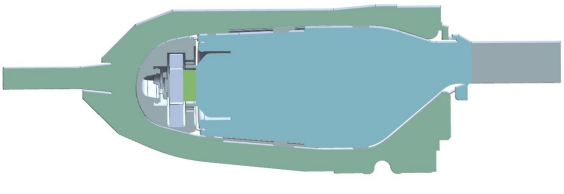

Fig. 6. Longitudinal cross-section of a solid-state mathematical flow model of a single-burner sector in a combustion chamber

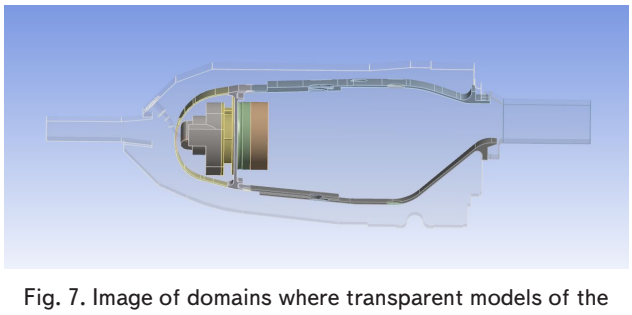

Fig. 7. Image of domains where transparent models of the working fluid flow part are depicted (fluid), and colored ones depict the simplified geometry of the real object (solid)

As a result of the CFD analysis, a graphical representation of the primary mesh (domain) and calculation stages was obtained (Fig. 8–12).

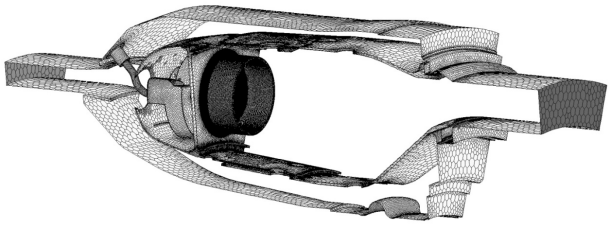

Fig. 8. Computational polyhedral mesh

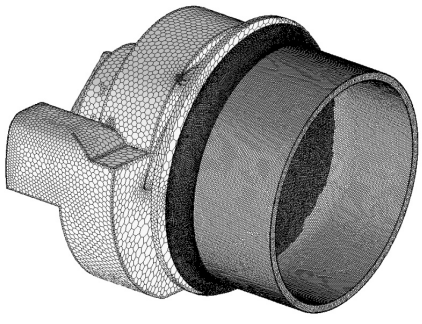

Fig. 9. Swirler calculation mesh

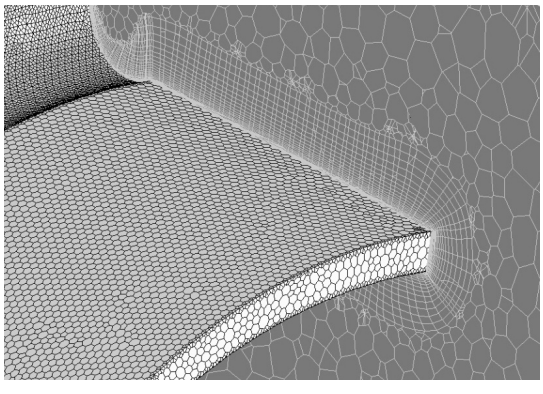

Fig. 10. Inflation area of the near-wall layer

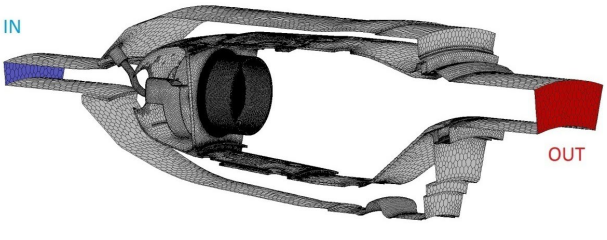

Fig. 11. Computational grid with boundary conditions

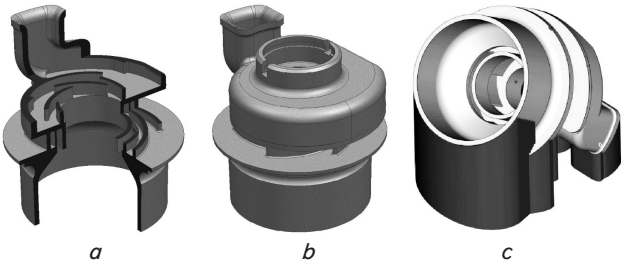

a *b* *c*

Fig. 12. Geometric representations of the swirler monopart: *a* — stepped cross-section, *b* — three-dimensional model of the swirler part, *c* — model of the swirler monopart with support

It was found that the constructed digital model with an optimized support system makes it possible to ensure the stability of geometric parameters during printing and minimize thermal deformations of the monopart.

The devised strategy for placing objects on the platform and the preparation of control SLI files form the necessary prerequisites for the transition to the direct implementation of the printing process using specific technological modes.

5. 2. Assessment of geometric accuracy and cost characteristics of manufactured swirler monoparts

The results of deviations from the 3D model of the swirler monopart manufactured by the additive method are shown in Fig. 13.

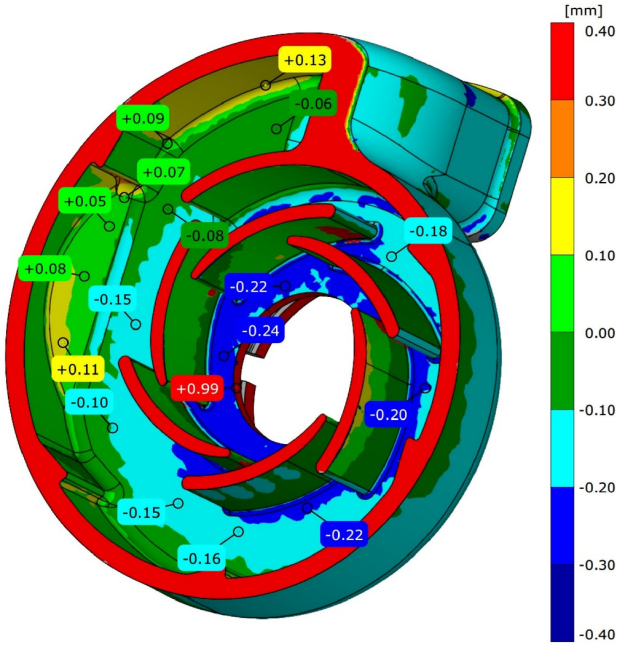

Fig. 13. Results of deviations in the geometric dimensions of the swirler manufactured by the additive method from the dimensions of the constructed three-dimensional model

The results confirmed that the geometry of the swirler blades manufactured using L-PBF technology corresponds to the three-dimensional model designed in Unigraphics NX.

To check the air flow rate through the air and fuel circuits, it is necessary to purge according to the scheme shown in Fig. 14.

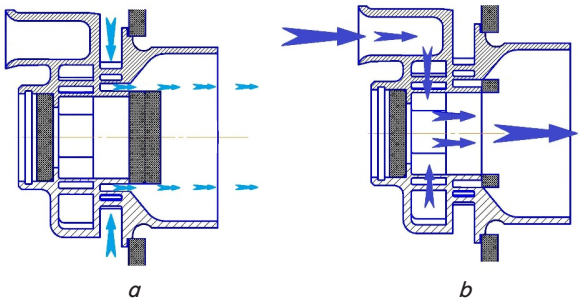

Fig. 14. Scheme of purging along the contours: *a* — along the air contour; *b* — along the fuel contour

Fig. 15, 16 show the results of checking the air flow along the contours of thirty swirlers.

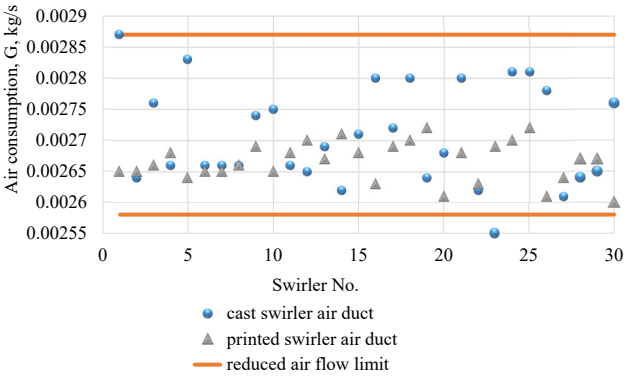

Fig. 15. Air flow test results for the air circuit

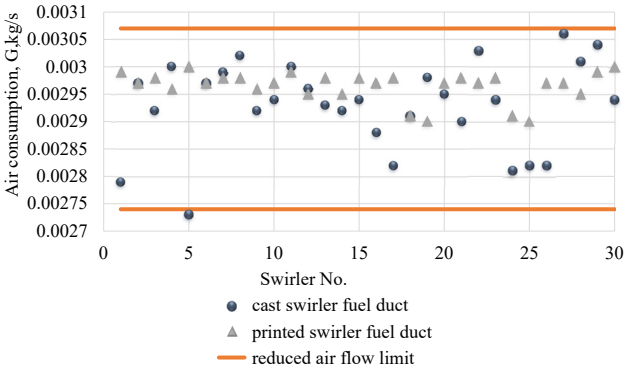

Fig. 16. Fuel circuit air flow test results

The results of checking the reduced air flow along the contours indicate that the air flow of swirlers manufactured by the conventional casting method is within the permissible limits but fluctuates throughout the tolerance field, several going beyond the limits. On the contrary, the results of checking the reduced air flow along the contours of a monopart manufactured using additive technology showed much better stability of the parameters.

After mechanical processing, the swirlers are subject to control and blowing of two contours simultaneously according to the scheme shown in Fig. 17.

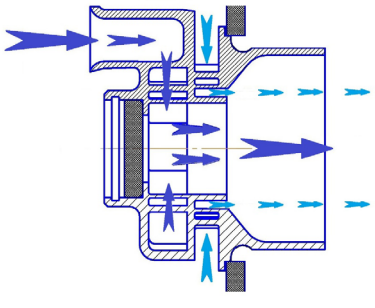

Fig. 17. Scheme for blowing two circuits simultaneously

The results of the total air flow rate along the contours are shown in Fig. 18.

The results of the purge show that the air flow rate along the contours of swirlers manufactured using conventional technology exceeds the permissible limit, while printed swirlers show more stable flow characteristics.

After control, swirlers are subject to assembly with a difference in the specified air flow rate in the set of no more than ±1.5%.

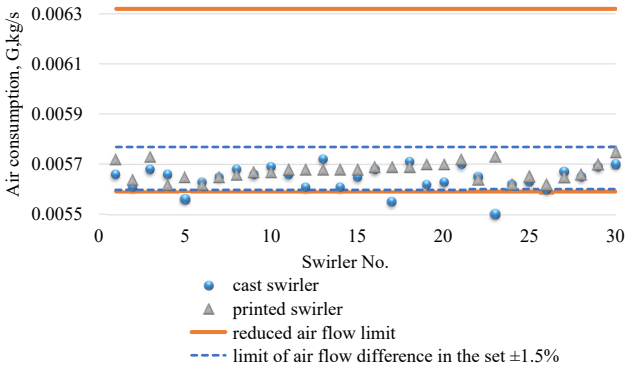

Fig. 18. Results of total air flow combined across circuits

Analysis of flow characteristics makes it possible to conclude that swirlers manufactured using conventional casting technology require more time for assembly than printed swirlers, which show more stable flow characteristics.

In order to determine the unevenness of the temperature field at the exit from the chamber, the combustion chamber was assembled and further tested using the above method before installation on the engine. The test volume was 5 cycles. The total duration of the tests was 30 minutes of continuous operation on the test bench.

Improving the stability of the air flow values in the set significantly affected the results of the combustion chamber tests regarding the distribution of the temperature field.

The maximum circular non-uniformity of the gas temperature field at the outlet of the combustion chamber τ_{max}, %, is defined as the relative deviation of the maximum temperature in the circumferential direction from the average mass temperature of the gas.

According to the results of the first test without additional corrections, the τ_{max} value was 12.51–18.91% with an allowable value of no more than 21%.

The low difference in the deviation of the air flow in the set of swirlers allowed for better mixing of fuel and air, forming a fuel-air mixture in the combustion zone of the combustion chamber. That had a positive effect on the circular non-uniformity of the temperature field.

Fig. 19 shows the temperature field, shape, length, and position of the flame, enriched combustion zones.

Fig. 20 depicts the thermal state of the swirler walls and the front part of the combustion chamber.

An inspection of the combustion chamber and swirlers showed that the combustion chamber and swirlers are in satisfactory condition (Fig. 21). No damage, deformations, or burnouts were found.

Qualification tests of an engine with a combustion chamber with installed swirlers manufactured using L-PBF technology using new materials, such as heat-resistant nickel-based alloys, were conducted; we show the results of defect detection (Fig. 22).

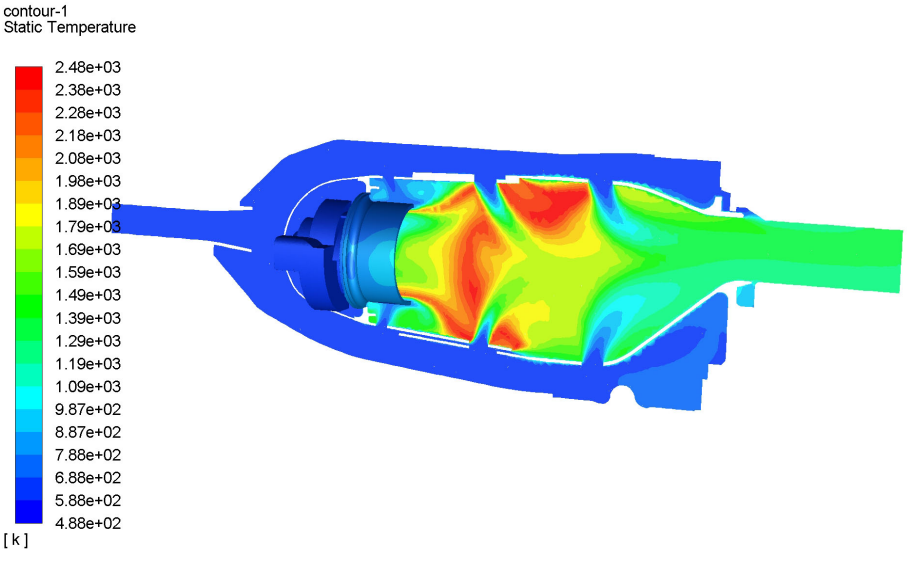

Fig. 19. Longitudinal cross-section along the axis of the temperature field swirler

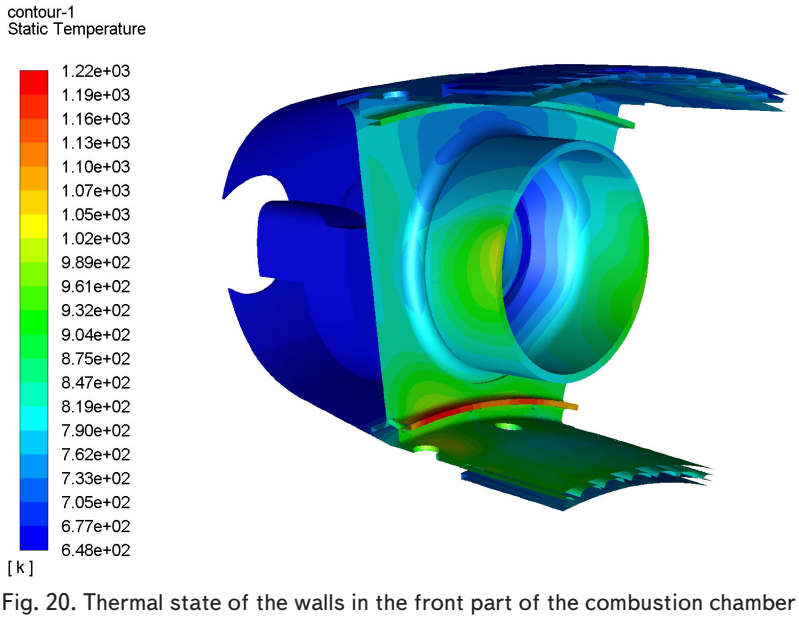

Fig. 20. Thermal state of the walls in the front part of the combustion chamber

Fig. 21. General view after combustion chamber temperature field tests

Fig. 22. General view of the combustion chamber and swirlers

Before installing the combustion chamber assembly on the engine, a control test is carried out to check the circumferential and radial unevenness of the temperature field at the outlet of the short-circuit in the plane of the nozzle apparatus. The test is carried out modularly on a specially equipped installation that simulates the engine operating mode in real conditions in a stationary mode.

During the tests, each thermocouple belt measures the temperature value at a given radius of the path, which corresponds to the control points (Table 3) of the radial unevenness diagram τ_{diagi} (Fig. 23). The vertical τ_{diagi} diagram of the gas temperature field at the outlet of the combustion chamber should not exceed that specified by the control points.

The calculation of points on the vertical τ_{diagi} diagram is carried out according to the following formula

$$\tau_{diagi} = \frac{t^*_{3ave_v} - t^*_{3ave.m}}{t^*_{3ave.m} - t^*_2} \times 100\%, \quad (4)$$

where $t^*_{3ave_v}$ is the average gas temperature measured in each zone at the outlet of the combustion chamber, °C

$$t^*_{3ave_v} = \frac{\sum t^*_{3i}}{n}, \quad (5)$$

where t^*_{3i} – measured at each point in the corresponding zone is the gas temperature at the outlet of the combustion chamber, °C; n is the number of temperature measurement points in the circumferential direction, but not less than 360; $t^*_{3ave.m}$ – mass average gas temperature at the outlet of the combustion chamber is calculated from the air flow rate G_{fl}, fuel flow rate G_f, and temperature t^*_3 at the completeness of combustion $\eta_c = 0.99$.

The $t^*_{3ave.m}$ calculation is performed according to the Ilyichov equation [9]

$$\frac{G_f}{G_{fl} \times 3600} = \frac{C_p\left(t^*_{3ave.m}\right) - C_p\left(t^*_2\right)}{H_u \times \eta_c - i\left(t^*_{3ave.m}\right) + C_p\left(t^*_2\right)}, \quad (6)$$

where H_u – low heat capacity of fuel, kcal; $C_p(t^*_{3ave.m}, t^*_2)$ – specific heat capacity of gas at temperature t, kcal/kg · K; $i(t^*_{3ave.m})$ – enthalpy of combustion products at temperature t, kcal/kg; t^*_2 – air temperature at the inlet to the combustion chamber, °C.

The maximum non-uniformity $\tau_{\max_i}$ of the gas temperature field at the outlet from the combustion chamber in each measurement zone should not exceed the value $\tau_{\max_i} = 21\%$

$$\tau_{\max_i} = \frac{t^*_{3\max_i} - t^*_{3ave.m}}{t^*_{3ave.m} - t^*_2} \times 100\%, \quad (7)$$

where $t^*_{3\max_i}$ – maximum temperature in each zone, °C.

Table 3

Position of thermocouple belts at the exit from CC relative to the path

Measurement belt number	τ_{diag}, %	Note
1	8	Outer wall of flow path
2	11.5	Intermediate cross-section of flow path
3	11.5	Middle of flow path
4	8	Intermediate cross-section of flow path
5	2	Inner wall of flow path

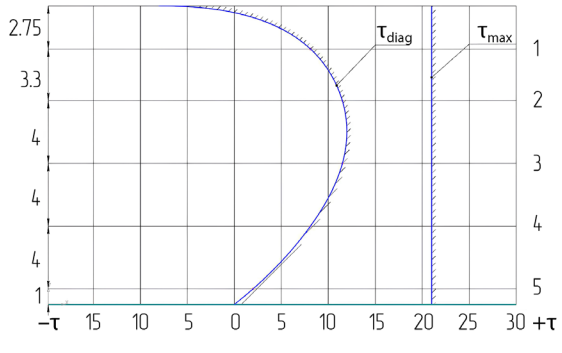

Fig. 23. Radial diagram of the flow part of the combustion chamber

If $\tau_{\max_i}$ exceeds the specified $\tau_{\max}$ values – the temperature field is corrected.

Reducing the maximum unevenness of the gas temperature field is achieved by reducing fuel consumption through individual nozzles of the main fuel collector. In cases where the permissible level of unevenness of the temperature field cannot be achieved, the swirler is replaced.

To determine the numbers of nozzles that need to be reduced in terms of fuel consumption, the temperature field processing procedure is performed:

1. On the horizontal sweep of the temperature field (Fig. 24), draw a line corresponding to the temperature at unevenness $\tau_{\max} = 21\%$ along all measurement zones. The zone with temperatures above the line exceeding $\tau_{\max}$ is called "hot". The points obtained from dividing the zones horizontally in half are

called "centers" of "hot" zones. The temperature values for $\tau_{\max_i} = 21\%$ are found from the following formula

$$t_{3_{\tau=21\%}} = 0/21 \times \left(t^*_{3ave.m} - t^*_2\right) + t^*_{3ave.m}. \quad (8)$$

2. Find the "centers" of the "hot" zones vertically on a horizontal line, on which the numbers of the swirlers and the corresponding numbers and axes of the nozzles (lines A, B) are indicated.

3. If the "centers" of the "hot" zones lag behind the axis of the nozzles by no more than 4° (nozzle vertical B), then the nozzle of the corresponding number is subject to correction for reducing fuel consumption by the amount of Y.

If the "centers" of the "hot" zones are located between the axes of the nozzles by more than 4° from each of them (nozzle vertical A), then both nozzles of the corresponding number are subject to correction by the amount of Y each.

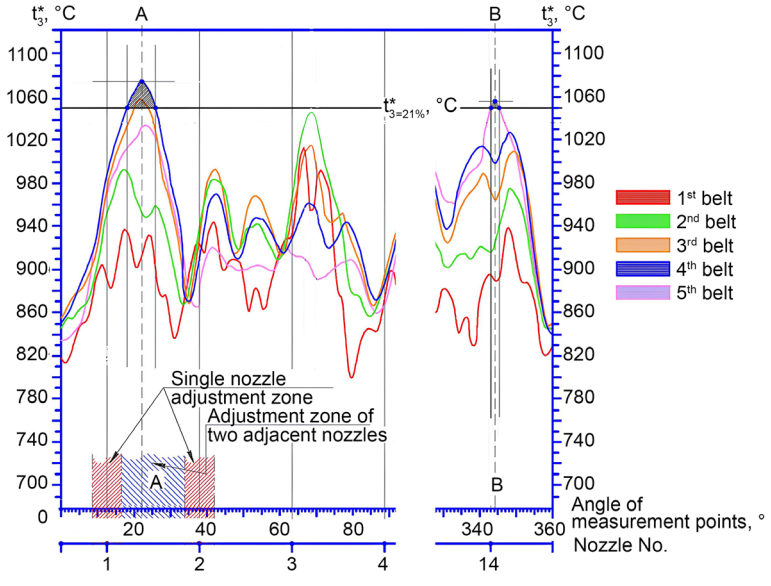

Fig. 24. Temperature field sweep

4. For each "hot" zone, the parameter X is determined, which is the ratio of the maximum (peak) temperature to the temperature corresponding to the non-uniformity $t_{3_{\tau=21\%}}$ according to the following formula

$$X = t^*_{3\max_i} / t_{3_{\tau=21\%}} \times 100\%. \quad (9)$$

5. The reduction in fuel consumption through the injectors that were subject to adjustment across all measurement zones is determined in percent

$$Y = 2\% + \left(X - 100\right) \times 2. \quad (10)$$

The resulting value is rounded up to the nearest whole percent. The maximum reduction in fuel consumption through one injector is no more than 26%.

The allowable value of the total change in fuel consumption (in percent) through the injector of the adjusted manifold is determined under the condition

$$\frac{[\sum Y]}{14} < 4\%, \quad (11)$$

where $[\sum Y]$ is the total value of the total correction of fuel consumption (in percent) for all adjusted nozzles.

In some cases, it is allowed, as an exception, to increase the fuel consumption of individual nozzles by $Y = 5\%$, if in the zone of this nozzle there is a "failure" in t^*_{3i} in the zone of not less than 40°C.

Blowing on the test bench showed that the spread of air flow characteristics along the contours does not exceed ±1.5%. This allowed us to eliminate the stage of careful selection of parts during assembly and ensured a uniform distribution of temperature fields in the combustion chamber, which was confirmed by successful qualification tests at VAT "MOTOR SICH" (Ukraine).

5. 3. Studying the influence of hot isostatic pressing on the structure of the material

Below are the results of our study on the influence of hot isostatic pressing (HIP) on the porosity and microstructure of the material for swirlers manufactured by the L-BPF additive method.

It is known that the additive manufacturing of parts is characterized by the presence of defects, in particular microporosity (up to ~ 10 μm), microdiscontinuities in the zones of fusion of layers, as well as oxide and carbide inclusions up to 15–30 μm in size, which is confirmed by the results of metallographic studies (Fig. 25).

Such defects are potential stress concentrators and can initiate fracture under conditions of cyclic thermal loads.

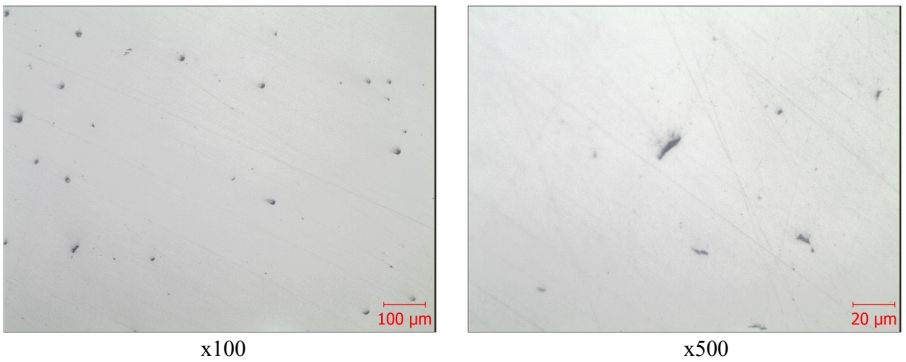

x100 x500

a *b*

Fig. 25. Microporosity in samples, before HIP: *a* — magnification x100; *b* — magnification x500 [17]

The parameters of HIP were as follows: temperature – 1040°C, pressure – 120 MPa (hold 1 hour) with subsequent heating to a temperature of 1150°C at a pressure of 160 MPa. After HIP, heat treatment (HT) was carried out according to the following modes: annealing at a temperature of 954°C (1 hour), aging at 718°C (8 hours), slow cooling in a furnace to a temperature of 621°C with a total hardening time of 18 hours.

According to the results of our studies, it was established that the use of hot isostatic pressing provides almost complete "healing" of internal pores and micro-discontinuities (Fig. 26), which is consistent with known literature data. The initial porosity of the material after L-BPF, which is 1.8–2.3%, after HIP decreases to values of about 0.2%, which indicates effective compaction of the structure.

Metallographic analysis revealed that in the initial state the material has a pronounced dendritic and layered structure of the γ-solid solution (Fig. 27), while after HIP and heat treatment its leveling and increase in homogeneity are observed (Fig. 28), the formation of strengthening phases, in particular γ''-afpb (Ni_3Nb), as well as δ-phase in the form of lamellar precipitates (Fig. 29), which corresponds to the top heat-treated state of the IN718 alloy.

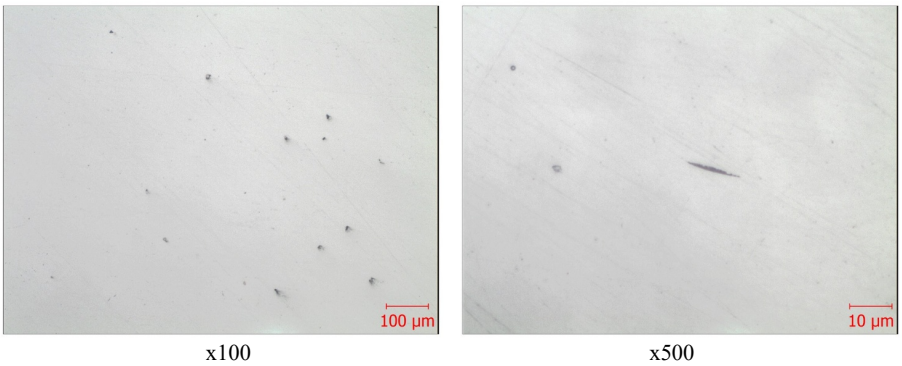

x100 x500

a *b*

Fig. 26. Zones of "healing" in samples, HIP+HT: *a* – magnification x100, *b* – magnification x500 [18]

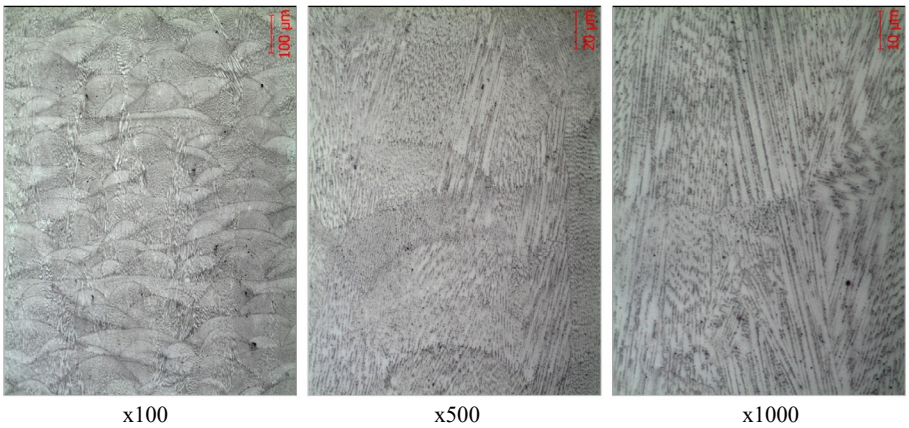

x100 x500 x1000

a *b* *c*

Fig. 27. Microstructure of no-heat-treated samples:
a – magnification x100; *b* – magnification x500; *c* – magnification x1000 [19]

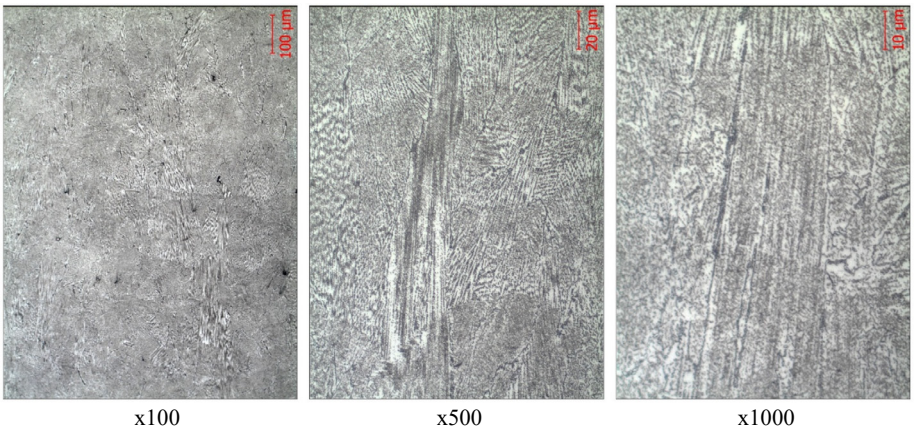

x100 x500 x1000

a *b* *c*

Fig. 28. Microstructure of heat-treated samples: *a* – magnification x100; *b* – magnification x500; *c* – magnification x1000 [19]

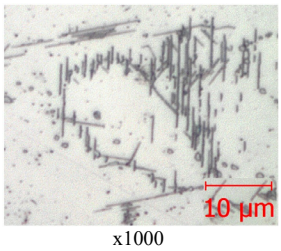

x1000

Fig. 29. Excess δ-phase magnification x1000 [18]

It was found that with an increase in the HIP pressure from 120 to 160 MPa, the degree of material densification increases from approximately 70% to over 90%, which indicates a significant influence of the process parameters on porosity. The results indicate that the use of HIP makes it possible:

– to reduce porosity and the number of internal defects;

– to increase the structural homogeneity of the material;

– to reduce the anisotropy of properties characteristic of L-BPF;

– to increase the reliability of parts under thermal load.

Thus, hot isostatic pressing is an effective technological stage that enables the formation of a stable and predictable material structure necessary for the operation of swirlers in aircraft gas turbine engines.

6. Discussion of results based on the study of gas-dynamic processes and the influence of additive manufacturing parameters on the functional accuracy of single-part swirlers

The calculated thermal state data (Fig. 24) showed that the average temperature of the swirler ring is 822 K, while local maxima in the inter-swirler nodes reach 1021 K. The obtained values slightly exceed the theoretical ones, which is explained by the complexity of mathematical modeling of combustion chambers with an evaporative fuel supply system. In particular, during a stationary calculation, it is difficult to take into account the dynamic change in the combustion start zone.

However, the coincidence of the outlet temperature (1264 K) with the real flight mode indicators (error within 2 degrees) confirms the adequacy of the chosen methodology for assessing the overall energy balance. This allowed us to proceed to the next stage – the implementation of the swirler design in metal.

Unlike conventional casting and subsequent soldering/welding of three separate parts (traditional method), the proposed solution is based on the manufacture of a single part using the L-PBF method from Inconel 718 powder.

The use of L-PBF technology for heat-resistant nickel alloys correlates with the successful experience by leading aerospace companies (Safran – Arrano and Ardiden-3 engines [20], Ariane Group – Ariane 6 nozzles [21], liquid jet engine injector [22], rocket nozzle [23], rocket engine [24]).

Unlike welded assemblies, where heat-affected zones are stress concentrators, a single part ensures the homogeneity of the structure. The use of the EOS M400 system made it possible to achieve complex internal geometry that cannot be realized by casting without increasing mass or losing accuracy [25].

3D scanning confirmed a smaller deviation from the digital model (Unigraphics NX) compared to the cast samples (Fig. 13). This directly affects the stability of the consumption characteristics: the absence of errors when soldering the contours guarantees the uniformity of the fuel-air mixture.

One of the key risks of L-PBF is residual porosity and gas inclusions (Fig. 25). The use of hot isostatic pressing (HIP) on the Quintus installation [26] allowed us to eliminate internal pores by plastic deformation and diffusion welding of surfaces under pressure. This provided mechanical properties at the level of the AMS 5662 standard, which is critical for operation at 1021 K. Unlike casting, where porosity is often an insurmountable defect, HIP in combination with L-PBF guarantees almost 100% material density.

Tests in the engine compartment confirmed the absence of deformations and burnouts, which proves the effectiveness of the selected material Inconel 718.

The proposed solution closes the problem of low resource and high error of the geometric parameters of welded swirlers.

Despite its advantages, our method requires laborious removal of support structures and mandatory HIP, which increases the cost of unit production. The internal channels after L-PBF have a higher roughness than after machining, which may affect the hydrodynamic resistance in the long term.

The study is limited to the dimensions of the EOS M400 camera.

Further research might aim at optimizing printing modes to reduce the number of support structures and studying the fatigue strength of the material under cyclic thermal loads that simulate engine start-stop modes.

7. Conclusions

1. A precision three-dimensional digital model of the combustion chamber swirler (including solid geometry and flow domains) was constructed in the Unigraphics NX environment. Based on this model, a comprehensive CFD analysis was performed with the construction of a polyhedral computational mesh and control SLI files were prepared for additive manufacturing (3D printing), which makes it possible to minimize thermal deformations of the monopart. Unlike standard models, this option contains an optimized support system that ensures stability of parameters compared to basic printing methods. This makes it possible to eliminate typical disadvantages of additive manufacturing – thermal deformations and deviations in the geometric parameters of the monopart. High accuracy and stability of the result are explained by the use of polyhedral meshes and special inflation zones (near-wall layers) during modeling, which ensures the correctness of CFD calculations. In addition, taking into account the strategy for placing objects on the printing platform at the design stage guarantees that the manufactured part complies with the mathematical model.

2. Analysis of our results from investigating the geometry of blades in the air and fuel-air circuit of the swirler using the 3D scanning method has established that in the vast majority of swirlers manufactured using conventional casting technology, there are deviations beyond the permissible tolerance field. The geometry of the swirler monopart manufactured using L-PBF technology is clearly within the specified tolerance field. Based on the analysis of our research results, it is shown that the geometric deviations in the internal surfaces of the contours led to a significant spread of consumption characteristics and rejection of 17% of the batch in total at all stages of post-processing. Printed

swirlers have more accurate geometric characteristics, which as a result stabilizes the difference in the indicated air flow rates both separately and together along the contours, which is fully within the assembly limits of ±1.5% and eliminates defects.

3. It was found that the initial porosity of the material, which after L-BPF is 1.8–2.3%, after HIP decreases to values of about 0.2%, which indicates effective compaction of the structure. Metallographic analysis revealed that after HIP and heat treatment, there is a leveling of the structure and an increase in its homogeneity, strengthening phases are formed. Accordingly, the reliability of parts under thermal load increases. Thus, hot isostatic pressing is an effective technological stage that enables the formation of a stable and predictable material structure necessary for the operation of swirlers in aircraft gas turbine engines.

Conflicts of interest

The authors declare that they have no conflicts of interest in relation to the current study, including financial, personal, authorship, or any other, that could affect the study and the results reported in this paper.

Funding

The study was conducted without financial support.

Data availability

The data will be provided upon reasonable request.

Use of artificial intelligence

The authors confirm that they did not use artificial intelligence technologies when creating the current work.

Authors' contributions

Volodymyr Yefanov: Supervision, Project administration**; Oleh Kalinichenko**: Conceptualization, Investigation, Writing – review & editing**; Dmytro Kuts**: Conceptualization, Methodology, Validation; **Oleh Ovchynnykov**: Investigation**,** Validation, Visualization**; Hanna Laptieva**: Methodology, Validation**,** Visualization.

References

1. Lefebvre, A. H., Ballal, D. R. (2010). Gas Turbine Combustion. CRC Press. https://doi.org/10.1201/9781420086058
2. Turns, S. R. (2012). An Introduction to Combustion: Concepts and Applications. McGraw-Hill, 736. Available at: https://www.academia.edu/40886924/An_Introduction_To_Combustion_Concepts_And_Applications_
3. Poinsot, T., Veynante, D. (2005). Theoretical and Numerical Combustion. R.T. Edwards, 540. Available at: https://www.researchgate.net/publication/248068931_Theoretical_and_Numerical_Combustion
4. Pitsch, H. (2006). Large-eddy simulation of turbulent combustion. Annual Review of Fluid Mechanics, 38 (1), 453–482. https://doi.org/10.1146/annurev.fluid.38.050304.092133
5. Lieuwen, T. C., Yang, V. (2006). Combustion Instabilities In Gas Turbine Engines. American Institute of Aeronautics and Astronautics. https://doi.org/10.2514/4.866807
6. Mattingly, J. D. (2002). Elements of Gas Turbine Propulsion. AIAA Education Series, 945. Available at: https://soaneemrana.org/onewebmedia/ELEMENTS%20OF%20GAS%20TURBINE%20PROPULTION2.pdf
7. Frazier, W. E. (2014). Metal Additive Manufacturing: A Review. Journal of Materials Engineering and Performance, 23 (6), 1917–1928. https://doi.org/10.1007/s11665-014-0958-z
8. Herzog, D., Seyda, V., Wycisk, E., Emmelmann, C. (2016). Additive manufacturing of metals. Acta Materialia, 117, 371–392. https://doi.org/10.1016/j.actamat.2016.07.019
9. Spierings, A. B., Herres, N., Levy, G. (2011). Influence of the particle size distribution on surface quality and mechanical properties in AM steel parts. Rapid Prototyping Journal, 17 (3), 195–202. https://doi.org/10.1108/13552541111124770
10. Vodennikova, O. S., Koval, M. O., Vodennikov, S. A. (2021). Investigation of Mechanical Properties and Structure of Inconel 718 Alloy Obtained by Selective Laser Sintering from Powder Produced by 'LPW'. Metallofizika I Noveishie Tekhnologii, 43 (7), 925–937. https://doi.org/10.15407/mfint.43.07.0925
11. Launder, B. E., Spalding, D. B. (1972). Lectures in Mathematical Models of Turbulence. London: Academic Press, 169.
12. Burke, S. P., Schumann, T. E. W. (1928). Diffusion Flames. Industrial & Engineering Chemistry, 20 (10), 998–1004. https://doi.org/10.1021/ie50226a005
13. Pope, S. B. (1976). The probability approach to the modelling of turbulent reacting flows. Combustion and Flame, 27, 299–312. https://doi.org/10.1016/0010-2180(76)90035-3
14. Crowe, C. T. (1982). Review – Numerical Models for Dilute Gas-Particle Flows. Journal of Fluids Engineering, 104 (3), 297–303. https://doi.org/10.1115/1.3241835
15. van Leer, B. (1997). Towards the Ultimate Conservative Difference Scheme. Journal of Computational Physics, 135 (2), 229–248. https://doi.org/10.1006/jcph.1997.5704
16. Turbomeca uses metal additive manufacturing for helicopter engine components. Available at: https://www.metal-am.com/turbomeca-uses-metal-additive-manufacturing-for-helicopter-engine-components/
17. Pedash, A. A., Klochykhin, V. V., Lysenko, N. A., Shilo, V. G., Kasay, P. A. (2019). Influence of the powder manufacturing technique on the structure and properties of the SLM-parts. Bulletin of Engine Building, 2, 31–39. Available at: https://www.google.com/url?sa=t&rct

=j&q=&esrc=s&source=web&cd=&ved=2ahUKEwjln6bLjo6UAxW9ywIHHX86JYgQFnoECBYQAQ&url=https%3A%2F%2Fvd.zp.edu.ua%2Farticle%2Fview%2F180255%2F180181&usg=AOvVaw1kuOs1mY5xtbSOyCCDmrKp&opi=89978449

18. Klochikhin, V. V., Kasai, P. A., Naumyk, V. V. (2022). Structure and Properties of Material of Samples, Cultivated by Selective Laser Melting of In718 Alloy Powder after Hot Isostatic Pressing and Subsequent Heat Treatment. Casting Processes, 147 (1), 19–29. https://doi.org/10.15407/plit2022.01.019
19. Klochikhin, V. V., Kasay, P. A., Balushok, K. B., Shilo, V. G., Naumyk, V. V. (2021). Study of the Material Quality of Samples Obtained by Selective Laser Melting (SLM) Method from IN718 Alloy Powder. Casting Processes, 144 (2), 12–22. https://doi.org/10.15407/plit2021.02.012
20. WZ16/Ardiden 3C. ENGINES. Safran-Group JSC. Available at: https://www.safran-group.com/products-services/ardiden-3c-first-jointly-developed-aero-engine-be-entirely-certified-china
21. Nozzles Ariane 6. Ariane-Group JSC. Available at: https://www.ariane.group/en/space-transportation/ariane-6/
22. Hahn, J. (2020). Hyperganic uses AI to design 3D-printed rocket engine. Available at: https://www.dezeen.com/2020/03/30/hyperganic-ai-rocket-engine-3d-printed/
23. 3D printing a rocket engine. Available at: https://www.etmm-online.com/3d-printing-arocket-engine-a-886960/
24. Giant Satellite Fuel Tank Sets New Record for 3-D Printed Space Parts. Available at: https://news.lockheedmartin.com/2018-07-11-Giant-Satellite-Fuel-Tank-Sets-New-Record-for-3-D-Printed-Space-Parts#assets_115
25. Yadroitsev, I., Yadroitsava, I., du Plessis, A., MacDonald, E. (2021). Fundamentals of Laser Powder Bed Fusion of Metals. Elsevier, 654. Available at: https://www.researchgate.net/publication/350007655_Fundamentals_of_Laser_Powder_Bed_Fusion_of_Metals
26. Kuts, D., Yefanov, V., Halienkova, O., Ovchynnykov, O., Tepla, T., Lemishka, I., Mierzwiński, D. (2025). Additive technologies for manufacturing swirlers of the combustion chamber of aircraft engines from nickel superalloy powders. Archives of Materials Science and Engineering. https://doi.org/10.5604/01.3001.0055.0368